

A structural study of ternary lanthanide orthoscamdate perovskites

Ruslan P. Liferovich¹ and Roger H. Mitchell*

Department of Geology, Lakehead University, 955 Oliver Road, Thunder Bay, Ont., Canada, P7B 5E1

Received 4 November 2003; received in revised form 6 February 2004; accepted 18 February 2004

Abstract

Ternary lanthanide scandates ($Ln=La, Pr, Nd, Sm, Eu, Gd, Tb, Dy, \text{ and } Ho$) have been synthesized at ambient pressure. Their structure has been investigated at room temperature by Rietveld analysis of powder X-ray diffraction data. The Ln -scandates are orthorhombic perovskites, adopting space group $Pbnm$ (# 62), $a \approx b \approx \sqrt{2}a_p$, $c \approx 2a_p$, $Z = 4$. Heavy lanthanides (Er–Lu), and Y do not form perovskites at ambient conditions. Compositionally driven phase transitions were not observed. The unit-cell parameters decrease with increasing ScO_6 octahedron rotation and atomic number of the Ln cation. In common with lanthanide orthoferrites, the uniform structural evolution is interrupted at the middle-heavy part of the lanthanide sequence. This is probably due to an interplay between: (i) enlargement of the ScO_6 octahedra relative to BO_6 in other perovskites (e.g., FeO_6 in $GdFeO_3$); (ii) reduction in size of the first coordination sphere of Ln^{3+} coincident with the lanthanide contraction; (iii) coincident expansion of the second coordination sphere due to screening effects of O^{1-} on O^{2-} , and entry of Sc to the lanthanide coordination sphere; (iv) complex mixing between oxygen and lanthanide f - and scandium d -orbitals. In the series studied, Ln^{3+} are in eight-fold coordination (tetragonal antiprism), and are considerably displaced from the center of the LnO_8 polyhedron along [001]. Evolution of the crystallochemical characteristics through the Ln orthoscamdate series is complex due to both the antipathetic distortions of A - and B -site coordination polyhedra and interaction of the orbitals of oxygen, Ln and Sc. Empirically obtained limits of Goldschmidt and observed t_o^{viii} tolerance factors for ternary $LnBO_3$ compounds adopting the $Pbnm$ structure are 0.795 and 0.841, respectively. © 2004 Elsevier Inc. All rights reserved.

Keywords: Lanthanide; Orthoscamdate; Perovskite; X-ray; Powder diffraction; Rietveld; Structure

1. Introduction

The study of stoichiometric ternary perovskite-type oxides of transition metals, $LnBO_3$, where Ln and B are trivalent lanthanides (rare earth elements) and first period transition metal cations, respectively, is of academic and industrial interest due to their relative ease of synthesis and wide variety of physical properties, e.g., metal–insulator transitions, anomalous magnetoresistance and catalytic properties [1,2], which can be modified by composition-driven structural variances.

The perovskite structure is well-known for permitting diverse ionic substitutions at all cationic sites due to its high tolerance to structural distortions [1]. In this respect the $LnBO_3$ perovskites display incremental

structural changes arising from the lanthanide contraction, i.e., the decrease of effective ionic radius with atomic number from $^{xii-viii}La^{3+}$ to $^{viii}Lu^{3+}$ [3], although the regularity of these changes is complicated for the mid-series lanthanides by diverse steric and electronic interactions [1,4,5].

Many of the $LnBO_3$ compounds adopt the $GdFeO_3$ -structure [4,6], which is isostructural with orthorhombic $CaTiO_3$, i.e., the perovskite structure *sensu stricto* [7–10]. The $GdFeO_3$ -structure is derived from the ideal ABO_3 cubic $Pm\bar{3}m$ aristotype by tilting of the FeO_6 octahedra about the [110] and [001] directions of the cubic subcell (Fig. 1) in response to the occupancy of the A -site by a lanthanide cation smaller than that required to form the ideal structure [1,7]. The octahedron tilting results in a reduction in symmetry to that of the $Pnma$ orthorhombic space group (#62). Most authors employ for $LnBO_3$ compounds adopting this space group the unconventional $Pbnm$ setting with $a \approx b \approx \sqrt{2}a_p$, $c \approx 2a_p$, $Z = 4$ [1,4]. The octahedron tilt scheme, expressed in Glazer's [11] notation, is $a^-a^-c^+$.

*Corresponding author. Fax: 807-346-7853.

E-mail address: Roger.Mitchell@lakeheadu.ca (R.H. Mitchell).

¹Permanent address: Geological Institute KSC RAS, 14 Fersmana Str., Apatity 184200, Russia.

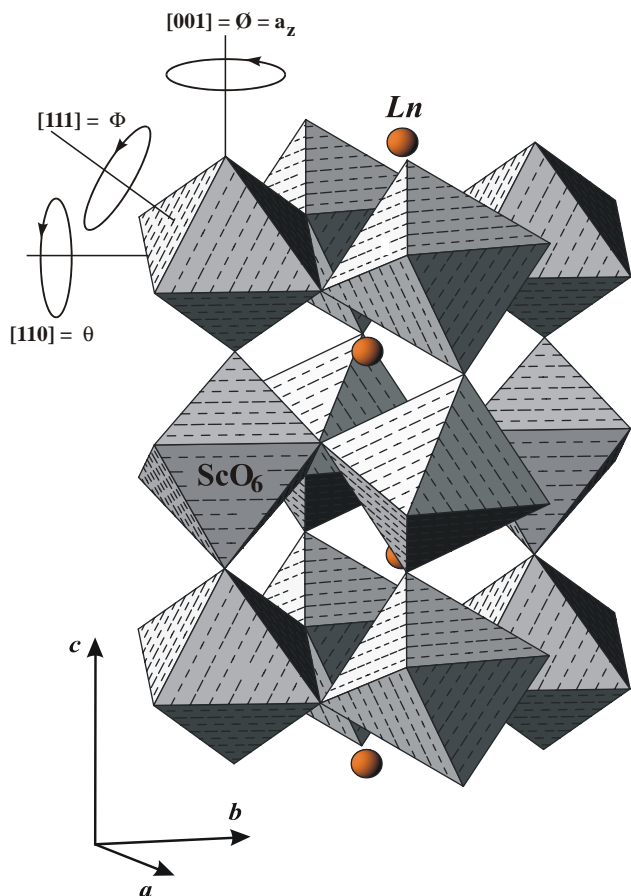


Fig. 1. Orthorhombic $LnScO_3$ crystal structure; ϕ , θ and Φ denote octahedron tilting about $[001]_p$, $[110]_p$, and $[111]_p$, respectively. Ln is a lanthanide (rare earth) atom in the A -site.

Curiously, the crystal chemistry of the lanthanide orthoperovskites, apart from the orthoferrites [7], has not been the subject of detailed investigation. The majority of studies of other orthorhombic compounds $LnBO_3$ ($B = Al, Ga, Sc, Ti, V, Cr, Co, Ni$) have reported data primarily for unit cell dimensions [12–14], and crystal structure determinations are limited to a few selected members of a given series of compounds rather than all of the possible lanthanide compounds, e.g., $LnCoO_3$ ($Ln = Pr, Nd, Sm, Tb, Dy, Ho,$ and Y) [15–18]; $LnNiO_3$ ($Ln = Pr, Nd, Sm, Eu, Gd, Dy$) [19–23]; $LnCrO_3$ ($Ln = Ce, La, Nd, Gd, Dy, Er,$ and Y) [24–32]; $LnTiO_3$ ($Ln = La, Nd, Sm, Gd$) [33]. Other $LnBO_3$ compounds have either not been synthesized or adopt rhombohedral symmetry, e.g., $R\bar{3}c$ $LnGaO_3$ and $LaAlO_3$ [34,35]. For the majority of the $LnBO_3$ orthoperovskites, the a and c unit cell dimensions have been found to decrease smoothly with increasing atomic number of the lanthanides, whereas the b dimension shows a more complex behavior, e.g., reaching maximum values at Gd–Tb–Dy in the orthoferrite series [4].

The $LnScO_3$ series, which are the subject of this work, have not been studied by modern methods. Initial

investigations [12,36–38] demonstrated that many (La–Tm) of the lanthanide scandates could be readily synthesized. Clark et al. [37] provided unit cell dimensions for $LnScO_3$ ($Ln = La, Nd, Sm, Gd, Dy, Ho, Er, Tm$), but were unable to synthesize $YbScO_3$ and $LuScO_3$. Unit cell data for the Ln -scandates prepared by Clark et al. [37] are not directly comparable throughout the series as the Ln ($= La, Nd, Sm, Gd$) compounds were formed in air at $1600^\circ C$ at ambient pressure, whereas the Ln ($= Dy, Ho, Er, Tm$) scandates were synthesized at 2.0 GPa at $1000^\circ C$. Crystal structure data with low accuracy and precision have been given for $EuScO_3$ by Faucher and Caro [39]. The only well-characterized structure is that of $GdScO_3$ [40].

It has been shown [1,4] that the coordination polyhedron of the lanthanides in the A -site of the orthorhombic perovskites is best regarded as $^{viii}[Ln^{3+}]$ rather than $^{xii}[Ln^{3+}]$, i.e., a four-fold anti-prism with $[2 \times O(1)$ and $6 \times O(2)]$ rather than a cubo-octahedron. This is because the rotation of the BO_6 octahedra to compensate for the poor fit of the lanthanides in the A -site results in the degeneration of 12 $Ln-O$ bonds to eight short $Ln-O$ and four long $Ln-O$ bonds, and determines the first and second coordination spheres for the Ln^{3+} cations. It has been suggested [4] that the degeneration of the coordination sphere is due to the antipathetic evolutionary trends of Ln -site bond lengths in the first and second coordination spheres. Bond valence analysis and crystal structure determinations [1,4] shows that the four long $Ln-O$ bonds exceed the $Ln-B$ distances in strongly distorted $LnBO_3$ orthoperovskites. The distortion of the lanthanide coordination polyhedron LnO_8 , is accompanied by a $[001]$ displacement of the lanthanide cation from the center of the polyhedron [1,4].

The objective of the present work was to synthesize a series of lanthanide orthoscaudates ($LnScO_3$) under uniform conditions and compare their crystal chemistry with that of the $LnFeO_3$ orthoferrite series, as the latter remain the best-characterized series of lanthanide orthoperovskites [4]. Our data are compared with those for other $LnBO_3$ orthoperovskites where appropriate.

Throughout the lanthanide orthoferrite series [1,4] the Goldschmidt tolerance factor [1,7] decreases smoothly from 0.926 to 0.860 for eight-fold coordinated La to Lu, respectively (Table 1). In this series, the LnO_8 polyhedral distortion, FeO_6 tilt angles and LnO_8/FeO_6 polyhedron volume ratios increase from the light (La) to heavy (Lu) lanthanides in accordance with the lanthanide contraction principle, apart from an anomaly at Gd [1,4]. In comparison to the LnO_8 polyhedra, the FeO_6 octahedra are less distorted with the maximum and minimum distortion occurring for $DyFeO_3$ and $GdFeO_3$, respectively [1].

Goldschmidt tolerance factors for $LnScO_3$ orthoperovskites are less than the majority of those of diverse

Table 1
Goldschmidt (t) and observed (${}^{\text{viii}}t_0$) tolerance factors for orthorhombic ternary lanthanide-transitional metal perovskites

	Al		Co		Fe		Ni		Cr		Ga		Sc		${}^{\text{vi}}\text{Ti}^{4+}$		
	${}^{\text{vi}}\text{R}_\text{B}^{3+}$	0.535	0.545 (low spin)		0.55 (low spin)		0.56 (low spin)		0.615		0.620		0.745		0.605		
${}^{\text{viii}}\text{Ln}^{3+}$	t	${}^{\text{viii}}t_0$	t	${}^{\text{viii}}t_0$	t	${}^{\text{viii}}t_0$	t	${}^{\text{viii}}t_0$	t	${}^{\text{viii}}t_0$	t	${}^{\text{viii}}t_0$	t	${}^{\text{viii}}t_0$	t	${}^{\text{viii}}t_0$	
La	1.160	(0.933)*	—	(0.928)*	—	0.926	0.918	(0.921)*	—	0.896	0.933	0.894	0.945	0.843	0.882	0.901	0.918
Pr	1.126	(0.921)*	—	(0.916)*	—	0.914	0.896	0.909	0.919	0.885	—	0.882	0.907	0.832	0.869	0.889	—
Nd	1.109	(0.915)*	—	0.910	0.913	0.908	0.888	0.903	0.916	0.879	0.895	0.877	0.899	0.826	0.862	0.883	0.884
Sm	1.079	0.904	0.931	0.899	—	0.897	0.875	0.892	0.894	0.868	—	0.866	—	0.816	0.853	0.873	0.846
Eu	1.066	0.899	—	0.895	—	0.892	0.871	0.888	0.887	0.864	—	0.862	—	0.812	0.850	0.868	—
Gd	1.053	0.894	—	0.890	—	0.888	0.868	0.883	0.881	0.859	0.883	0.857	0.875	0.808	0.853	0.864	0.856
Tb	1.040	0.890	0.898	0.885	0.876	0.883	0.862	0.879	—	0.855	—	0.853	—	0.803	0.852	0.859	—
Dy	1.027	0.885	—	0.881	0.895	0.878	0.858	0.874	0.868	0.850	0.869	0.848	—	0.799	0.847	0.854	—
Ho	1.015	0.881	0.892	0.876	0.869	0.874	0.855	0.870	0.883	0.846	—	0.844	—	0.795	0.841	0.850	—
Er	1.004	0.877	—	0.872	—	0.870	0.851	0.866	—	0.842	0.863	0.840	—	0.792	—	0.846	—
Tm	0.994	0.873	—	0.869	—	0.866	0.849	0.862	—	0.839	—	0.837	—	0.788	—	0.843	—
Yb	0.985	0.870	—	0.865	—	0.863	0.845	0.859	—	0.836	—	0.834	—	0.785	—	0.840	—
Lu	0.977	0.867	—	0.863	—	0.860	0.843	0.856	—	0.833	—	0.831	—	0.783	—	0.837	—

Note. Ln a lanthanide cation; ${}^{\text{viii}}\text{Ln}^{3+}$ and ${}^{\text{vi}}\text{R}_\text{B}^{3+}$ cationic radii of a lanthanide and a transitional metal in eight- and six-fold coordination, respectively, Å [3].

— No data available.

(0...)* values for the compounds adopting trigonal symmetry.

LnBO_3 orthoperovskites (Table 1), suggesting that orthoscamdates might form highly distorted structures, e.g., the Goldschmidt tolerance factor of LaScO_3 (0.843) is less than that (0.86) of the most-distorted orthoferrite LuFeO_3 . The low tolerance factors of the heavy lanthanide scandates (<0.8) suggest that they might form perovskite structures of lower symmetry or compounds having an entirely different structure. The latter possibility is certainly indicated by the experiments of Clark et al. [37] which led to the synthesis of cubic $(\text{Yb,Sc})_2\text{O}_3$ and $(\text{Lu,Sc})_2\text{O}_3$ solid solutions with $Ia\bar{3}$ symmetry [41,42] rather than orthoperovskites.

2. Experimental

Lanthanide orthoscamdates were synthesized from stoichiometric amounts of the relevant oxides (high purity grade; Alfa Aesar Chemical Co.). The Tb oxide was characterized as Tb_7O_{12} (PDF # 85-1801) by powder X-ray diffractometry. This and Pr_7O_{12} were reduced with 5 wt% of graphite powder at the calcination stage. All reagents were dried at 120°C and mixed in an agate mortar under acetone, followed by calcination in air for 24 h at 1000°C. After regrinding, the samples were pelletized at a pressure of 10 tonnes per square centimeter, and then heated in air for nine days at 1475°C, with regrinding and pelleting every two days. Step-scanned X-ray diffraction (XRD) powder patterns of the products were obtained at room temperature using a Philips 3710 diffractometer ($\text{CuK}\alpha$ radiation; 2θ range 10°–145°; $\Delta 2\theta$ step 0.02°; time per step 2 s).

The XRD patterns were inspected using the Bruker AXS software package EVA to identify the phases present and confirm that perovskite-structured compounds were present. Data were further analyzed by Rietveld methods using the Bruker AXS software package TOPAS version 2.1 operated in the fundamental parameters mode [43]. This recently introduced Windows-based software provides significant improvements in the ease of undertaking Rietveld refinements over commonly used DOS-based software such as FULLPROF [44]. Results obtained by either of these programs are similar. Depending upon the presence of impurities the number of TOPAS 2.1 refined variables ranged from 46 to 67 independent parameters. These included: zero corrections; scaling factors; Lorentz polarization corrections; cell dimensions; atomic positional coordinates; preferred orientation corrections; crystal size and strain effects; and isotropic thermal parameters (B_{iso}). Fig. 2 is a Rietveld refinement plot for EuScO_3 . Isotropic thermal parameters were in some instances fixed at values given in the literature for other lanthanide perovskites [19,22] as in our refinements B_{iso} became close to zero. Fixing B_{iso} did not result in significant changes to the atomic coordinates.

The ATOMS-6.0 software package [45] was used to determine interaxial angles describing the distortion of ScO_6 octahedra, i.e., the $\text{Sc-O}(1)\text{-Sc}$ and $\text{Sc-O}(2)\text{-Sc}$ angles. The IVTON program [46] was employed to characterize the coordination spheres of Ln and Sc , obtain bond lengths, volumes of coordination polyhedra and displacements of cations from the centers of

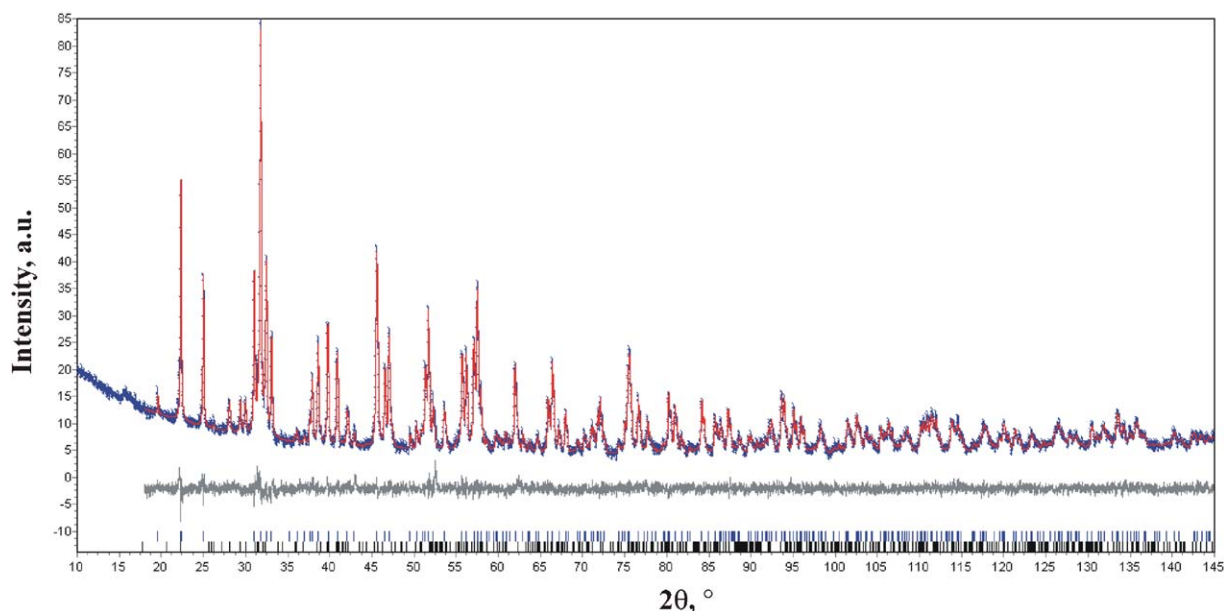


Fig. 2. Rietveld refinement plot of the X-ray powder diffraction data for EuScO_3 at room temperature. The bars indicate the allowed Bragg reflections for EuScO_3 (upper) and $(\text{Eu}, \text{Sc})_2\text{O}_3$ solid solution (lower). For details of the refinement, see text and Table 2.

coordination polyhedra. Tilt angles of ScO_6 octahedra were calculated from bond angles following Zhao et al. [47].

The compositions of samples were determined by X-ray energy-dispersion spectrometry (EDS) using a JEOL JSM-5900 scanning electron microscope (SEM) equipped with a LINK ISIS 300 analytical system incorporating a Super ATW Element Detector (133 eV FWHM MnK). Raw EDS spectra were acquired for 130 s (live time) with an accelerating voltage of 20 kV, and beam current of 0.475 nA on nickel metal. The spectra were processed with the LINK ISIS-SEMQUANT software package, with full ZAF corrections applied. The $L\alpha$ -lines were used with standardization on natural loparite for La, Ce, Pr and Nd, on individual lanthanide fluorides for Sm, Eu, Gd, Tb, Dy and Ho and metallic Sc for Sc.

Most of the experimental products contained small quantities of starting materials (Table 2) which do not exceed 5–7 vol% according to SEM BSE data. XRD and EDS analyses of the run products indicated that the impurity phases were either Ln_2O_3 and Sc_2O_3 or solid solutions of cubic $(\text{Ln}, \text{Sc})_2\text{O}_3$. Accurate assessment of the amount present is precluded by the extensive overlap of the XRD reflections of $Pbnm$ -perovskite and minor oxide phases. For example, the (004) reflection of TbScO_3 overlaps with the (60 $\bar{3}$) reflection of cubic $(\text{Sc}, \text{Ln})_2\text{O}_3$; the (110) reflection of EuScO_3 overlaps with (202) of Eu_2O_3 and (211) of Sc_2O_3 , etc. The compositions of the lanthanide scandates were found to be close to stoichiometry regardless of the presence of small amounts of the impurities.

3. Results and discussion

At ambient pressure and temperature, orthoscaandates were formed by La, Pr, Nd, Sm, Eu, Gd, Tb, Dy and Ho. In this series, the ionic radius of Ln^{3+} in eight-fold coordination decreases from 1.16 Å ($^{\text{viii}}\text{La}^{3+}$) to 1.015 Å ($^{\text{viii}}\text{Ho}^{3+}$) [3]. Consequently, Goldschmidt tolerance factors [7] for these lanthanides in combination with $^{\text{vi}}\text{Sc}^{3+}$ (0.745 Å) range from 0.843 to 0.795 (Table 1). Experiments with smaller cations such as $^{\text{viii}}\text{Y}^{3+}$ (1.019 Å, $t = 0.797$) and the heavy lanthanides ($^{\text{viii}}\text{Ln}^{3+} = 1.004\text{--}0.977$ Å, $t = 0.792\text{--}0.783$) did not produce perovskites at ambient conditions. Attempts to form these compounds by high-pressure synthesis ($P = 6$ GPa, $T = 1200^\circ\text{C}$, $t = 8$ h) produced a mixture with less than 50 vol% of $Pbnm$ ErScO_3 perovskite, and complex mixtures of cubic phases for Tm, Yb, Lu, and Ce. These data confirm previously published studies on the instability of orthoscaandates of the heavy lanthanides at $P > 2$ GPa [37].

We performed multiple syntheses of GdScO_3 , TbScO_3 and DyScO_3 under the same conditions to confirm our crystallochemical data. The cell dimensions, fractional atomic coordinates and isotropic temperature factors (Table 2) of each compound were reproduced within the statistical limits in each experiment. Thus, we conclude the anomalous evolution trends of the crystallochemical characteristics of middle lanthanide orthoscaandates (see below) not to be due to any errors related to preparation and processing of the initial mixtures.

For the Rietveld refinement, we used the atomic coordinates given by Marezio et al. [4] for $Pbnm$ -

Table 2
Crystallographic characteristics of lanthanide orthoscatandates

	La	Pr	Nd	Sm	Eu	Gd	Tb	Dy	Ho
a (Å)	5.6803(1)	5.6118(1)	5.5809(1)	5.5343(1)	5.5109(1)	5.4862(1)	5.4654(1)	5.4494(1)	5.4295(1)
b (Å)	5.7907(1)	5.7802(1)	5.7765(1)	5.7622(1)	5.7565(1)	5.7499(1)	5.7292(1)	5.7263(1)	5.7148(1)
c (Å)	8.0945(1)	8.0276(1)	8.0072(1)	7.9674(1)	7.9515(1)	7.9345(1)	7.9170(1)	7.9132(1)	7.9011(1)
V (Å ³)	266.253(7)	260.394(6)	258.134(6)	254.078(5)	252.251(6)	250.299(5)	247.900(5)	246.932(5)	245.162(5)
$Ln: x_A$	0.0100(2)	0.0117(2)	0.0128(2)	0.0146(2)	0.0157(2)	0.0163(2)	0.0164(2)	0.0172(2)	0.0175(2)
Y_A	0.9572(1)	0.9500(1)	0.9474(1)	0.9431(1)	0.9417(2)	0.9406(2)	0.9405(2)	0.9393(2)	0.9385(1)
Z_A	$\frac{1}{4}$	$\frac{1}{4}$	$\frac{1}{4}$	$\frac{1}{4}$	$\frac{1}{4}$	$\frac{1}{4}$	$\frac{1}{4}$	$\frac{1}{4}$	$\frac{1}{4}$
d_A	0.502	0.455	0.435	0.402	0.379	0.374	0.367	0.367	0.363
Δx_A	−0.0007	−0.0009	−0.0002	0.0018	0.0026	0.0021	0.0019	0.0029	0.0029
Δy_A	0.0867	0.0787	0.0752	0.0698	0.0659	0.0649	0.0640	0.0641	0.0634
$B(\text{Å}^2)$	0.32(2)	0.88(2)	0.12(2)	0.12(2)	0.21(2)	0.30(2)	0.38(3)	0.35(2)	0.32(2)
Sc: x_B	0	0	0	0	0	0	0	0	0
Y_B	$\frac{1}{2}$	$\frac{1}{2}$	$\frac{1}{2}$	$\frac{1}{2}$	$\frac{1}{2}$	$\frac{1}{2}$	$\frac{1}{2}$	$\frac{1}{2}$	$\frac{1}{2}$
Z_B	0	0	0	0	0	0	0	0	0
$B(\text{Å}^2)$	0.70(4)	0.70(4)	0.70(4)	0.70(4)	0.70(4)	0.70(5)	0.70(5)	0.70(4)	0.70(4)
O1: x	0.9032(15)	0.9034(16)	0.8944(17)	0.8882(17)	0.8802(16)	0.8817(17)	0.8798(16)	0.8804(15)	0.8804(11)
Y	0.5277(14)	0.5375(16)	0.5427(17)	0.5488(19)	0.5556(17)	0.5535(18)	0.5551(18)	0.5550(15)	0.5561(12)
Z	$\frac{1}{4}$	$\frac{1}{4}$	$\frac{1}{4}$	$\frac{1}{4}$	$\frac{1}{4}$	$\frac{1}{4}$	$\frac{1}{4}$	$\frac{1}{4}$	$\frac{1}{4}$
$B(\text{Å}^2)$	1.00(8)	1.00(8)	1.00(8)	1.0(1)	1.0(1)	1.0(1)	1.0(1)	1.00(9)	1.0(1)
O2: x	0.7073(11)	0.6996(12)	0.6983(12)	0.6986(13)	0.6976(12)	0.6931(13)	0.6918(13)	0.6926(11)	0.6916(8)
Y	0.2958(11)	0.3021(12)	0.3039(13)	0.3056(14)	0.3021(13)	0.3007(14)	0.2993(14)	0.3040(12)	0.3054(9)
Z	0.9479(9)	0.9439(9)	0.9427(9)	0.9394(10)	0.9405(9)	0.9444(10)	0.9436(10)	0.9392(8)	0.9339(6)
$B(\text{Å}^2)$	1.00(8)	1.00(8)	1.00(8)	1.0(1)	1.0(1)	1.0(1)	1.0(1)	1.00(9)	1.0(1)
R_{wp}	12.18	13.54	13.01	12.89	12.00	12.11	11.49	12.10	10.48
R_{exp}	8.44	9.65	9.17	9.74	9.46	8.72	8.08	8.66	6.77
R_{Bragg}	3.24	4.21	3.98	3.61	3.13	3.81	4.00	4.69	3.23
GoF	1.44	1.40	1.42	1.32	1.27	1.39	1.42	1.40	1.55
DW	1.08	1.15	1.13	1.25	1.34	1.17	1.17	1.16	0.96
$R_2O_3\%$	2.4(2) ^a	2.4(3) ^a	≤5 ^b	≤7 ^b	≤7 ^b	6.0(8) ^a	≤7 ^b	4.8(5) ^a	6.9(6) ^a
$LnScO_3\%$	97.6(2) ^a	97.6(3) ^a	≥95 ^b	≥93 ^b	≥93 ^b	94.0(1) ^a	≥93 ^b	95.2(6) ^a	93.1(6) ^a

Note. Standard deviations are given in parentheses. Δx_A and Δy_A Parameters in fractions of the unit cell dimensions (a, c) describing displacement of A -site cation from the center of coordination polyhedron, d_A (Å).

R_2O_3 mixture of Ln_2O_3 , Sc_2O_3 and $(Ln, Sc)_2O_3$ remaining non-reacted in 9 days at 1475°C (see text for details). B -factors for Sc, O1, and O2 fixed at values similar to those in the literature [19,22].

^aRietveld refinement data.

^bEstimated using SEM BSE scanning technique.

structured $GdFeO_3$ as a starting model. The atomic coordinates and crystallochemical characteristics of the Ln -orthoscatandates synthesized are given in Tables 3 and 4, and illustrated in Figs. 3–7. Data for $GdScO_3$ agree well with previous data for this compound given by Amanyan et al. [40]. In common with Ln -orthoferrites [4], the orthorhombic distortion of the Ln -orthoscatandates increases parallel to the lanthanide contraction. In contrast to the Ln -orthoferrites [4], which exhibit anomalous b lattice parameters for Gd–Dy [1], the orthoscatandates do not exhibit any anomalies with respect to change in the b lattice parameter as a function of composition (Fig. 3).

All of the Ln -orthoscatandates have $a < c/\sqrt{2} < b$ (Fig. 3) and $f - 12 = V_{A12}/V_B < 5$ (Table 4). Such “non-reversed” lattice parameters suggest that distortion of the coordination polyhedra are sufficient to overcome the contraction in the a -dimension resulting from tilting. Thus, none of these compounds are close to second-

order phase transitions at ambient pressure and temperature.

As expected for these strongly distorted perovskite structures, the A -site coordination polyhedron is a four-fold antiprism (C.N.=8). The Δ_8 distortion indices of the AO_8 coordination polyhedra (or polyhedron bond length distortion, according to [3,1], $\Delta_8 = 1/n \sum \{(r_i - r)/r\}^2 \times 10^3$, where r_i and r are individual and average bond lengths, respectively) in most of the Ln -orthoscatandates are nearly twice those described in their orthoferrite counterparts (Fig. 4b; Table 4), and other $LnBO_3$ perovskites (see Table 3.2 in [1]). On the whole, the Δ_8 distortion increases in the orthoscatandates following the lanthanide contraction which results in decreasing size of the AO_8 polyhedron and reduction in the mean A –O bond lengths in the first coordination sphere (Fig. 4c; Table 3). This overall trend is complicated for the middle lanthanides as only a slight decrease from SmO_8 ($\Delta_8 = 7.380$) to EuO_8 ($\Delta_8 = 7.367$)

Table 3
Selected interatomic distances (Å) and angles (°) in lanthanide orthoscatandates

	La	Pr	Nd	Sm	Eu	Gd	Tb	Dy	Ho
<i>Ln</i> -O1	2.382(9)	2.384(9)	2.338(10)	2.311(10)	2.278(9)	2.278(9)	2.331(10)	2.266(8)	2.262(6)
<i>Ln</i> -O1	2.560(9)	2.461(9)	2.429(10)	2.377(11)	2.345(10)	2.345(10)	2.263(9)	2.324(9)	2.309(7)
2 × <i>Ln</i> -O2	2.423(7)	2.364(7)	2.349(7)	2.326(8)	2.340(7)	2.352(8)	2.343(8)	2.306(7)	2.269(5)
2 × <i>Ln</i> -O2	2.700(7)	2.678(7)	2.663(7)	2.617(7)	2.600(7)	2.617(8)	2.603(7)	2.585(6)	2.559(5)
2 × <i>Ln</i> -O2	2.894(7)	2.859(7)	2.851(7)	2.854(8)	2.843(7)	2.801(8)	2.799(7)	2.820(6)	2.847(5)
<i>Ln</i> -O1	3.358(9)	3.321(9)	3.354(10)	3.560(11)	3.393(10)	3.365(10)	3.364(10)	3.349(9)	3.337(7)
<i>Ln</i> -O1	3.359(9)	3.449(9)	3.501(10)	3.360(11)	3.611(10)	3.600(10)	3.600(10)	3.604(9)	3.607(7)
2 × <i>Ln</i> -O2	3.575(7)	3.639(7)	3.366(7)	3.680(8)	3.664(7)	3.648(8)	3.641(7)	3.679(6)	3.710(5)
2 × Sc-O1	2.103(2)	2.090(3)	2.101(3)	2.105(3)	2.119(3)	2.110(3)	2.109(3)	2.107(3)	2.104(2)
2 × Sc-O2	2.083(6)	2.086(7)	2.080(7)	2.066(7)	2.073(7)	2.075(8)	2.059(8)	2.073(6)	2.077(5)
2 × Sc-O2	2.121(6)	2.123(7)	2.125(7)	2.113(8)	2.106(7)	2.084(7)	2.088(7)	2.089(7)	2.098(5)
2 × O1-Sc-O2	88.3(3)	86.9(3)	87.3(3)	86.8(3)	85.7(3)	85.5(3)	85.4(3)	86.3(3)	86.1(2)
2 × O1-Sc-O2	89.1(3)	88.9(3)	87.9(3)	87.3(3)	87.3(3)	88.2(3)	88.2(3)	87.2(3)	87.4(2)
2 × O1-Sc-O2	90.9(3)	91.1(3)	92.1(3)	92.7(3)	92.7(3)	91.8(3)	91.8(3)	92.8(3)	92.7(2)
2 × O1-Sc-O2	91.7(3)	93.1(3)	92.7(3)	93.2(3)	94.3(3)	94.5(3)	94.6(3)	93.7(3)	93.9(2)
2 × O2-Sc-O2	91.4(4)	91.2(4)	91.1(4)	91.2(4)	90.8(4)	90.0(4)	90.1(4)	90.5(4)	91.0(3)
2 × O2-Sc-O2	88.6(4)	88.8(4)	88.9(4)	88.8(4)	89.3(4)	90.0(4)	89.9(4)	89.5(4)	89.0(3)
δ	1.6	3.5	3.7	5.5	7.5	6.7	6.9	6.0	6.7
O1-Sc-O1	180	180	180	180	180	180	180	180	180
Sc-O1-Sc	148.39	147.56	144.60	144.22	139.48	140.19	139.57	139.80	139.73
Sc-O2-Sc	149.45	146.26	145.45	142.32	144.91	145.64	145.38	143.50	141.52

Note. δ Bond angle variance (see text and [1] for explanation).

Table 4
Crystal chemistry of lanthanide orthoscatandates

	<i>AO</i> ₈	<i>A</i> ₈	<i>A</i> -O(1)	<i>A</i> -O(2)	<i>BO</i> ₆	<i>A</i> ₆	<i>B</i> -O	<i>f</i> -8	Δ <i>V</i>	<i>AO</i> ₁₂	<i>f</i> -12	[110]	[001]	[111]	<i>a</i> _x ⁻
La	29.038(14)	5.469	2.622(7)	3.467(7)	12.380(7)	0.055	2.102(4)	2.34	25.15	54.18	4.38	15.81	10.44	18.87	11.21
Pr	28.068(14)	6.020	2.581(7)	3.512(7)	12.320(7)	0.062	2.100(5)	2.28	24.71	52.78	4.28	16.22	12.42	20.33	11.51
Nd	27.578(14)	6.592	2.562(7)	3.397(7)	12.363(8)	0.076	2.102(6)	2.22	24.59	52.17	4.22	17.70	11.95	21.25	12.57
Sm	26.896(14)	7.380	2.535(9)	3.570(9)	12.321(8)	0.096	2.101(6)	2.18	24.30	51.20	4.16	17.89	14.03	22.59	12.70
Eu	26.631(12)	7.367	2.524(8)	3.583(8)	12.284(8)	0.085	2.099(6)	2.17	24.15	50.78	4.13	20.26	10.13	22.55	14.40
Gd	26.570(14)	6.344	2.520(8)	3.565(8)	12.122(8)	0.050	2.090(4)	2.19	23.88	50.45	4.16	19.91	9.85	22.12	14.15
Tb	26.294(14)	6.608	2.511(8)	3.561(8)	12.044(8)	0.097	2.085(6)	2.16	23.64	49.93	4.15	20.22	9.75	22.36	14.37
Dy	26.015(11)	7.596	2.502(7)	3.578(7)	12.122(7)	0.044	2.089(5)	2.14	23.60	49.61	4.09	20.10	11.47	23.03	14.29
Ho	25.694(9)	9.008	2.490(6)	3.591(6)	12.177(5)	0.031	2.093(4)	2.11	23.42	49.11	4.03	20.14	12.99	23.82	14.31

Crystal chemistry of lanthanide orthoferrites [1,4]

La	27.535	3.056	2.605	—	10.761	0.003	2.006	2.56	22.46	49.99	4.65	11.83	7.72	14.09	8.38
Pr	26.482	3.207	2.546	3.280	10.795	0.008	2.008	2.45	22.25	48.73	4.51	13.39	9.83	16.55	9.49
Nd	26.119	3.349	2.527	3.316	10.833	0.007	2.011	2.41	22.18	48.30	4.46	14.34	10.13	17.49	10.16
Sm	25.411	3.882	2.493	3.370	10.866	0.040	2.013	2.34	21.99	47.40	4.36	15.55	11.09	19.02	11.03
Eu	25.121	3.941	2.479	3.392	10.867	0.038	2.013	2.31	21.87	46.99	4.32	16.12	11.29	19.59	11.43
Gd	24.922	3.882	2.469	3.411	10.856	0.032	2.012	2.30	21.77	46.69	4.30	16.51	11.33	19.93	11.71
Tb	24.523	4.433	2.453	3.420	10.841	0.047	2.012	2.26	21.59	46.11	4.25	17.09	11.74	20.64	12.13
Dy	24.244	4.667	2.442	3.435	10.848	0.059	2.012	2.23	21.47	45.72	4.21	17.48	12.16	21.18	12.41
Ho	23.959	4.882	2.430	3.443	10.813	0.054	2.010	2.22	21.31	45.27	4.19	17.98	12.12	21.57	12.77
Er	23.722	5.271	2.421	3.455	10.833	0.038	2.011	2.19	21.20	44.92	4.15	18.63	12.13	22.12	13.23
Tm	23.556	5.660	2.414	3.463	10.830	0.029	2.011	2.18	21.28	44.68	4.13	18.95	12.20	22.42	13.46
Yb	23.247	6.030	2.402	3.472	10.820	0.029	2.011	2.15	20.97	44.21	4.09	19.33	12.64	22.96	13.76
Lu	23.052	6.584	2.395	3.474	10.807	0.030	2.010	2.13	20.08	43.88	4.06	19.65	12.75	23.29	13.97

Note. *AO*₈ and *AO*₁₂ volumes (Å³) of polyhedra with *A*-site cation in eight- and twelve-fold coordination, respectively.

*BO*₆ is the volume (Å³) of the *ScO*₆ polyhedron. *A*₈ and *A*₆ are the distortion indices of the *AO*₈ and *BO*₆ polyhedra, respectively.

*AO*₁₂ the ideal volume of the *A*-site polyhedron which is calculated from *V* and *BO*₆. *A*-O¹ and *B*-O are the mean bond lengths (Å) for the *AO*₈ and *BO*₆ polyhedra, respectively, *A*-O(1) first and *A*-O(2) second coordination spheres of lanthanide ion. The volume of the second coordination sphere, Δ*V*, is *AO*₁₂-*AO*₈. Polyhedron volume ratios (*V*_A/*V*_B), *f*-12 and *f*-8, are for eight- and twelve-fold coordinated *A*-site cations, respectively. [110], [001] and [111] are octahedral tilts angles (°) and *a*_x⁻ is the [100]=[010] tilt angle (°); all tilt angles are determined from bond angles.

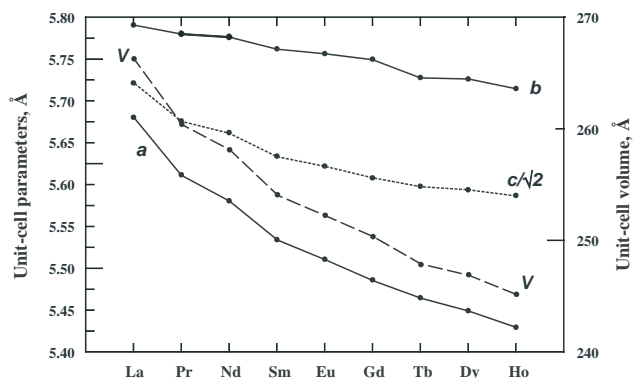


Fig. 3. Variation in unit-cell parameters and volumes in lanthanide orthoscatandates.

is observed. The GdO_8 and TbO_8 antiprisms are not extensively distorted ($\Delta_8 = 6.344$ and 6.608 , respectively; Table 4; Fig. 4b).

Regardless of the fluctuations of AO_8 volume throughout the series, the volume of the second coordination sphere ($\Delta V_{O12} = AO_{12} - AO_8$, Table 4; Fig. 4a) decreases very smoothly throughout the lanthanide orthoscatandate series. The relative decrease in size of the second coordination sphere of the Ln -orthoscatandates (Fig. 4a) is greater than that observed for orthoferrites. Incomplete data available for orthogallates, orthotitanates and other $LnBO_3$ perovskites show the opposite trend of increasing ΔV_{O12} towards perovskites based on heavier lanthanides [1]. The variation of the [001]-displacement of the lanthanide cation from the center of LnO_8 coordination polyhedron decreases rapidly from La to Eu and rather smoothly for Gd–to–Ho (Fig. 7a).

One should expect distortion of the ScO_6 octahedron (Δ_6) to be not especially dependent on the radii of the lanthanide cations in the A -site. However, there appears to be a quite complex relationship (Fig. 5b; Table 4), as Δ_6 increases for orthoscatandates of (La–Sm) and irregularly decreases in the Eu–Ho orthoscatandates. The latter show a poorly developed trend of decreasing Δ_6 values towards the heavier lanthanides. The least-distorted ScO_6 octahedra in $EuScO_3$ and $GdScO_3$ demonstrate the highest bond angle (δ) variances (Fig. 6), where $\delta = \Sigma[(\theta_i - 90)^2 / (n - 1)]$ [1]. The Sc–O bond lengths vary coincidentally with ScO_6 -volumes (Figs. 5a and c), being greatest in $NdScO_3$ and least in Gd, Tb, and Dy orthoscatandates. In common with Δ_8 variations, which have a minimum at $GdScO_3$ (Fig. 4a), distortion indices of the ScO_6 octahedra (Δ_6) decrease drastically at $GdScO_3$, but are high for $TbScO_3$, lower for $DyScO_3$ and minimal for $HoScO_3$ (Fig. 5b; Table 4), the smallest of the lanthanide ions adopting the ScO_6 -based perovskite structure. These observations are in part correlated with Δ_6 distortion indexes calculated for Ln -orthoferrites [4,1], and follow variations observed for this series with higher orders of magnitude in the range

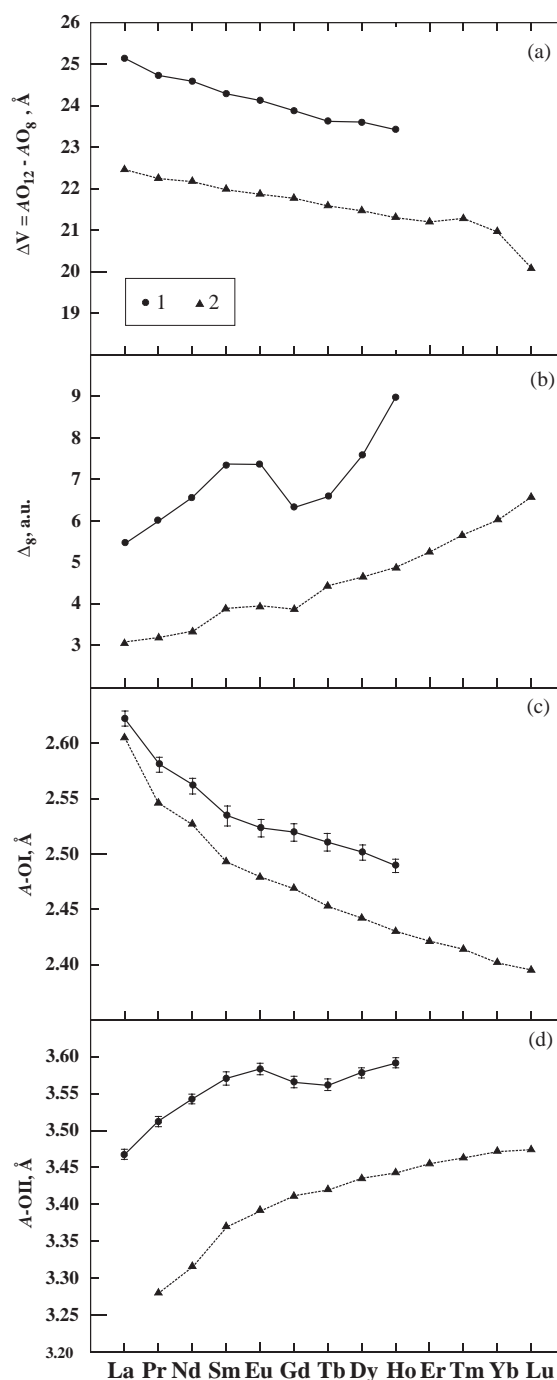


Fig. 4. Characteristics of a lanthanide coordination polyhedra (AO_8 tetragonal antiprism) in lanthanide orthoperovskites. 1 Lanthanide orthoscatandates; 2 Lanthanide orthoferrites.

from La to Tb, but are lower for $DyScO_3$ and $HoScO_3$ (Fig. 5b). The Δ_6 distortion indexes of the BO_6 octahedron in the light lanthanide- and Tb-orthoscatandates are the largest yet found for lanthanide-transitional metal perovskites in which Jahn-Teller distortion is absent. We consider that the anomalous Δ_6 distortion of $TbScO_3$ might be a result of partial oxidation of Tb

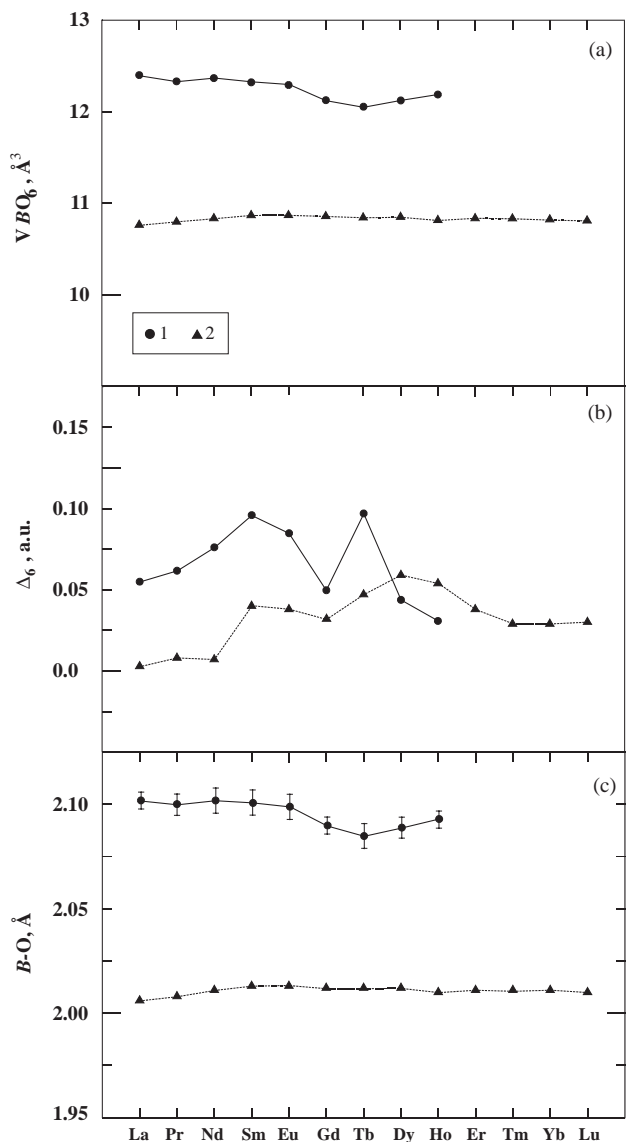


Fig. 5. Characteristics of a transitional metal coordination polyhedron (BO_6 octahedra) in lanthanide orthoperovskites. 1 Lanthanide orthoscatdates; 2 Lanthanide orthoferrites.

during synthesis. The decrease in ionic radius following oxidation to Tb^{4+} ($r = 0.76 \text{\AA}$) could result in the entry of small amounts of Tb to the Sc-site. Such Sc–Tb diadochy might affect bond lengths but not the BO_6 volume (Table 4, Fig. 5) and observed tolerance factor (Table 1). Oxidation of Tb might be a common problem during the synthesis of $TbBO_3$ compounds as shown by anomalous average Al–O bond length of the AlO_6 polyhedron in $TbAlO_3$ (1.911 \AA) relative to that of $SmAlO_3$ (1.899 \AA) and $SmAlO_3$ (1.907 \AA) [48–50].

Polyhedron volume ratios, V_A/V_B , decrease irregularly throughout the lanthanide scandates series both for AO_8 and AO_{12} volumes ($f-8$ and $f-12$, respectively; Table 4), with a significant decrease for the La–Sm compounds and a rather limited one for Eu–Ho (Figs. 7b and c).

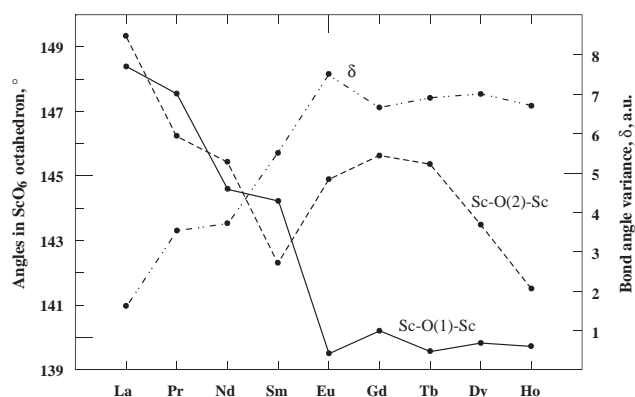


Fig. 6. Variation of bond angles in ScO_6 octahedra.

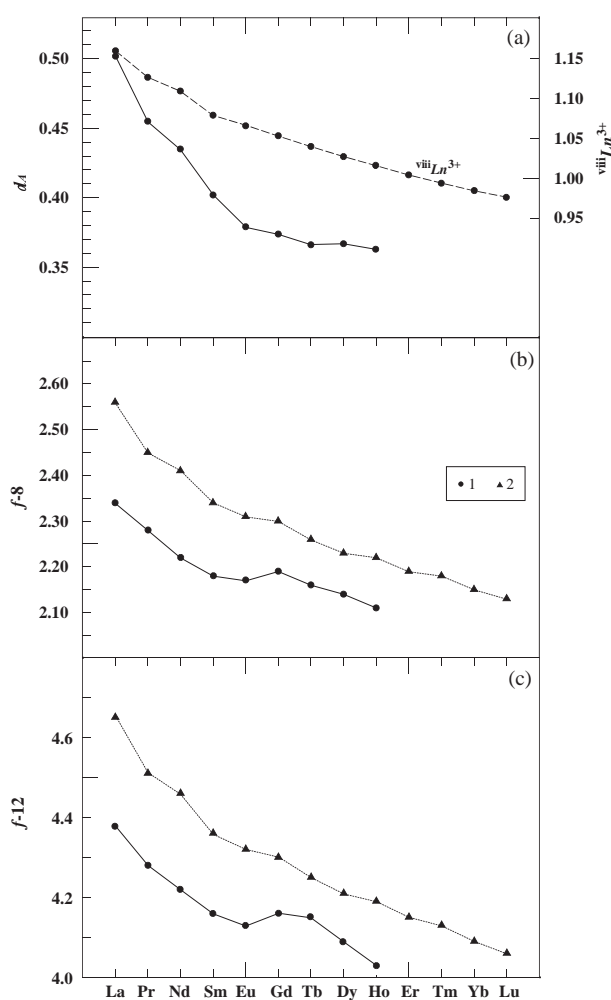


Fig. 7. (a) Vector components of a lanthanide ion displacement from the central position in coordination polyhedra (AO_8 tetragonal antiprism); (b) Ratios of polyhedron volumes for AO_8 ($f-8$) and AO_{12} ($f-12$). 1 Lanthanide orthoscatdates; 2 Lanthanide orthoferrites.

Eu–Tb orthoscatdates behave anomalously in showing no decrease of either $f-8$ or $f-12$ with atomic number, whereas $GdScO_3$ demonstrates anomalously high ratios.

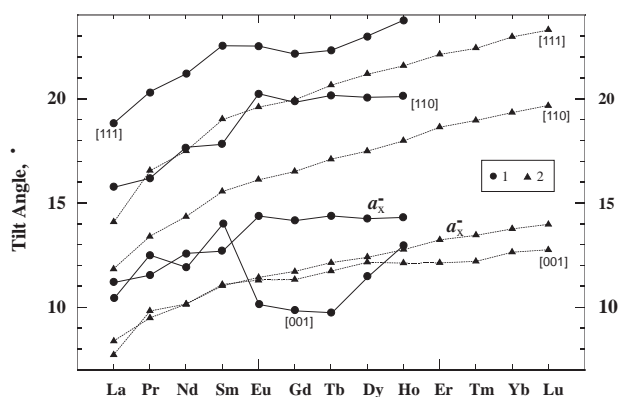


Fig. 8. Tilt angles for lanthanide orthoscatandates series as compared to lanthanide orthoferrites. 1 orthoscatandates; 2 orthoferrites; 3 orthoaluminates; 4 orthogallates; 5 orthotitanates; 6 orthochromates.

Table 4 and Fig. 8 show the changes in the ScO_6 tilt angles throughout the orthoscatandate series. The anomalously low value of the [111] tilt for the Gd and Eu–Tb compounds, respectively, is coincident with the changes determined for Δ_8 , $A\text{--O}(1)$ and Δ_6 (Figs. 4a and b). As the polyhedral volume changes reflect principally the effects of the [110] tilts, the latter are coincident with the V_A/V_B variations (Figs. 7b and c), and show an anomaly for EuScO_3 , GdScO_3 , and TbScO_3 . The most irregular trend is that of the [001] octahedron tilt angles, which show a rapid decrease at EuScO_3 , further slow decrease at GdScO_3 to a minimum at TbScO_3 , followed by increased values for Dy–Ho orthoscatandates.

Marezio et al. [4] have formulated empirical reasons for the anomalous crystallochemical characteristics of middle lanthanide-transitional metal orthoperovskites, nevertheless a quantitative model describing these anomalies has not yet been developed. Marezio et al. [4] noted that among the 12 $A\text{--O}$ distances in the lanthanide orthoperovskites, the bond lengths in the first coordination sphere decrease coincidentally with the lanthanide contraction, whereas $A\text{--O}$ distances for the second coordination sphere increase (Figs. 4c and d). The increase of the second nearest neighborhood bond lengths is ascribed to “the screening effect of the first-nearest oxygen atoms on the second-nearest oxygen atoms” [4] (the atom in the B -site, entering the second coordination sphere, also provides screening effect). The second reason for the anomaly occurs when $Ln\text{--O}(2)$ bond lengths became considerably longer than that those of $Ln\text{--}B$, resulting in B -cations lying closer to the lanthanide ion in A -site than the four $\text{O}(2)$ atoms. This steric effect occurs in the ternary lanthanide-transitional metal perovskites with the least-distorted BO_6 polyhedra in the GdFeO_3 structure due to the relatively small radii of the transition element cations present (Fe^{3+} (l.s.), Co^{3+} (l.s.), Ni^{3+} (l.s.), Al^{3+} , and Rh^{4+}). In the orthoscatandates, this regularity is obviously complicated by the larger radius of ${}^{\text{vi}}\text{Sc}^{3+}$ as compared to those of

${}^{\text{vi}}\text{Fe}^{3+}$, ${}^{\text{vi}}\text{Ti}^{4+}$ and ${}^{\text{vi}}\text{Rh}^{4+}$, and thus considerably larger BO_6 octahedron volumes and longer bond lengths (Figs. 5a and c; Table 4, [1,4]). Nevertheless, this does not explain the non-coincidence of the anomalous distortion of AO_8 and ScO_6 (Δ_8 and Δ_6 , respectively). Most probably, this is due to complex mixing between oxygen and lanthanide f - and scandium d -orbitals coupled with gross size differences in the A -site cations along the series and distortion of the enlarged BO_6 polyhedron. These effects probably interfere in the middle-lanthanide part of the series with size changes being dominant for the light lanthanides and orbital mixing for the middle-heavy lanthanides [1,4]. In the case of TbScO_3 , the partial oxidation of the terbium during high-temperature synthesis in air might be one more reason for departure from the trend expected by the lanthanide contraction.

4. Conclusions

The series of lanthanide orthoscatandates from La to Ho have been synthesized at ambient pressure in air by ceramic techniques and their structures have been determined by Rietveld refinement of powder X-ray diffraction at room temperature. These ternary stoichiometric perovskites, in common with GdFeO_3 and CaTiO_3 , adopt space group $Pbmn$, and contain distorted coordination polyhedra of both Ln and Sc ions, together with strongly tilted ScO_6 octahedra. Our experimental data extend the range of $Ln\text{ScO}_3$ compounds adopting the $Pbmn$ perovskite structure at ambient pressure from La–Gd [37], to La–Ho, and support the data of [37] that the small lanthanides (Y, Er–Lu) do not adopt perovskite structures at low or high pressures.

Because of the decrease in size of lanthanides through the series investigated, the Goldschmidt tolerance factor

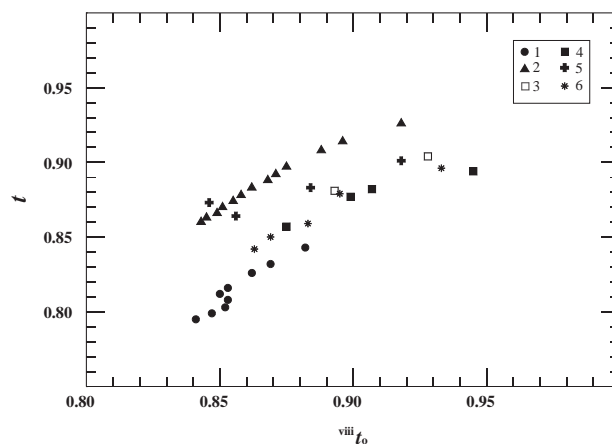


Fig. 9. Plot of observed tolerance factors (${}^{\text{viii}}t_o$) versus Goldschmidt tolerance factor (t) for diverse ternary lanthanide-transitional metal perovskites.

decreases from 0.843 (LaScO₃) to 0.783 (hypothetical LuScO₃) (Fig. 9). The empirically found “critical value” of this parameter for the stability limits of a *Ln*-orthoscamdate perovskite at ambient pressure must lie between 0.795 (HoScO₃, the most distorted but stable orthoscamdate synthesized), and 0.792 (for hypothetical ErScO₃). In terms of the observed tolerance factor, t_{0}^{viii} [1], the critical distortion of perovskite structure in the scandates is just less than $t_{0}^{viii} = 0.841$ (t_{0}^{viii} observed in HoScO₃, Table 1). Our data confirm the anomalous distortion of coordination polyhedra and average bond lengths observed for GdScO₃ [40].

Our data show no composition-driven phase transitions in the lanthanide orthoscamdates prepared. The evolution of their crystallochemical characteristics throughout the series is complicated by interference of the antipathetic distortions of the *A*- and *B*-site coordination polyhedra and interaction of the electron orbitals of oxygen, lanthanides and Sc, and probably partial oxidation in the case of Tb.

Acknowledgments

This work is supported by the Natural Sciences and Research Council of Canada and Lakehead University. Mr. Alan MacKenzie is acknowledged for assistance with the X-ray diffraction and SEM EDS microprobe work, Mrs. Anne Hammond is warmly thanked for help with preparation of samples.

References

- [1] R.H. Mitchell, *Perovskites: Modern and Ancient*. Almaz Press, Thunder Bay, Ontario, Canada, 2002, 322pp (<http://www.almazpress.com>).
- [2] B. Wishwanathan, *J. Sci. Ind. Res.* 43 (1984) 151.
- [3] R.D. Shannon, *Acta Crystallogr. A* 32 (1976) 751.
- [4] M. Marezio, J.P. Remeika, P.D. Dernier, *Acta Crystallogr. B* 26 (1970) 2008.
- [5] J. Pérez-Cacho, J. Blasco, J. García, R. Sanchez, *J. Solid State Chem.* 150 (2000) 145.
- [6] S. Geller, *J. Chem. Phys.* 24 (1956) 1236.
- [7] V.M. Goldschmidt, *Skrifter Norsk. Vidensk. Akad. Klas. I* (1926) 2.
- [8] S.V. Náráy-Szabó, *Naturwissenschaften* 31 (1943) 202.
- [9] I. Náráy-Szabó, *Pub. of Univ. of Tech. Sci., Budapest*, Vol. 1, 1947, p. 30.
- [10] H.D. Megaw, *Nature* 155 (1945) 484.
- [11] A.M. Glazer, *Acta Crystallogr. B* 28 (1972) 3384.
- [12] S. Geller, *Acta Crystallogr.* 10 (1957) 243.
- [13] S. Geller, P.J. Curlander, G.F. Ruse, *Mater. Res. Bull.* 9 (1974) 637.
- [14] M. Marezio, J.P. Remeika, P.D. Dernier, *Inorg. Chem.* 7 (1968) 1337.
- [15] H.W. Brinks, H. Fjellvag, A. Kjekshus, B.C. Hauback, *J. Solid State Chem.* 147 (1999) 464.
- [16] H. Taguchi, *J. Solid State Chem.* 122 (1996) 297.
- [17] A. Kappatsch, S. Quezel-Ambrunaz, J. Sivardiere, *J. Phys.* 31 (1970) 369.
- [18] A. Mehta, R. Berliner, R.W. Smith, *J. Solid State Chem.* 130 (1997) 192.
- [19] J.L. García Muñoz, J. Rodríguez-Carvajal, P. Lacorre, J.B. Torrance, *Phys. Rev. B.* 46 (1992) 4414.
- [20] P. Lacorre, J.B. Torrance, J. Pannetier, A.I. Nazzari, P.W. Wang, T.C. Huang, *J. Solid State Chem.* 91 (1991) 225.
- [21] G. Demazeau, A. Marbeuf, M. Pouchard, P. Hagenmueller, *J. Solid State Chem.* 3 (1971) 582.
- [22] J.A. Alonso, M.J. Martínez-Lope, I. Rasines, *J. Solid State Chem.* 120 (1995) 170.
- [23] J.A. Alonso, M.J. Martínez-Lope, M.T. Casais, M.A.G. Aranda, M.T. Fernández-Díaz, *J. Am. Chem. Soc.* 121 (1999) 4754.
- [24] A. Wold, R. Ward, *J. Am. Chem. Soc.* 76 (1954) 1029.
- [25] E.F. Bertraut, J. Mareschal, *J. Solid State Chem.* 5 (1967) 93.
- [26] Z.A. Zaitseva, A.L. Litvin, S.S. Ostapenko, *Dopovidi Akad. Nauk Ukr. RSR B* (1977) 1094.
- [27] C.P. Khattak, D.E. Cox, *Mater. Res. Bull.* 12 (1977) 463.
- [28] H. Taguchi, M. Nagao, Y. Takeda, *J. Solid State Chem.* 114 (1995) 236.
- [29] H. Taguchi, *J. Solid State Chem.* 118 (1995) 367.
- [30] Z.A. Zaitseva, A.L. Litvin, *Dopovidi Akad. Nauk Ukr. RSR B* 994 (1978).
- [31] B. van Laar, J.B.A.A. Elemans, *J. Phys.* 32 (1971) 301.
- [32] J.T. Looby, L. Katz, *J. Amer. Chem. Soc.* 76 (1954) 6029.
- [33] D.A. Maclean, H.N. Ng, J.E. Greedan, *J. Solid State Chem.* 30 (1979) 35.
- [34] W. Marti, P. Fischer, F. Altorfer, H.J. Scheel, M. Tadin, *J. Phys.: Condens. Matter* 6 (1994) 127.
- [35] C.J. Howard, B.J. Kennedy, *J. Phys.: Condens. Matter* 11 (1999) 3229.
- [36] W. Trzebiatowski, R. Horyn, *Z. Chem.* 5 (9) (1965) 347.
- [37] J.B. Clark, P.W. Richter, L.Du. Toit, *J. Solid State Chem.* 23 (1–2) (1978) 29.
- [38] J.E. Greedan, K. Seto, *Mater. Res. Bull.* 16 (1981) 1479.
- [39] M. Faucher, P. Caro, *Mater. Res. Bull.* 10 (1975) 1.
- [40] P.A. Amanyan, E.V. Antipov, V.A. Antonov, P.A. Arsenyev, *Russ. J. Inorg. Chem.* 32 (1987) 1225.
- [41] A. Saiki, N. Ishizawa, N. Mizutani, M. Kato, *J. Ceram. Soc. Japan* 93 (1985) 649.
- [42] T. Schlied, G. Myer, *J. Less Common Metals* 149 (1989) 73.
- [43] A.A. Kern, A.A. Coelho, Allied Publishers Ltd., Karlsruhe, 144 (1998). <http://www.bruker-axs.com>
- [44] J. Rodríguez-Carvajal. FULLPROF 2000. Laboratoire Léon Brillouin (CEA/CNRS), Cea-Saclay, France, 2000.
- [45] E. Dowty, *Atoms 5.0*, By Shape Software, Kingsport, TN 37663, USA, 1999.
- [46] T. Balić, Žunić, I. Vicković, *I. Appl. Crystallogr.* 29 (1996) 305.
- [47] Y. Zhao, D.J. Weidner, J.B. Parise, D.E. Cox, *Phys. Earth Planet. Interiors* 76 (1993) 1.
- [48] M. Marezio, P.D. Dernier, J.P. Remeika, *J. Solid State Chem.* 4 (1972) 11.
- [49] A. Bombik, B. Lesniewska, J. Mayer, A. Oles, A.W. Pacyna, J. Przewoznik, *J. Magn. Mater.* 168 (1997) 139.
- [50] A.A. Levin, *Kristallografiya* 37 (1992) 1020.